Thermodiffusion-induced instabilities in reactive systems

Sumana Dutta and Deb Shankar Ray*
Indian Association for the Cultivation of Science, Jadavpur, Calcutta 700 032, India
(Received 17 January 2007; revised manuscript received 6 March 2007; published 18 June 2007)

We examine the influence of a thermal gradient on a classical reaction-diffusion system. The different instability regions in the appropriate parameter space are examined. We show how the imposed temperature gradient destabilizes a chemical front via the Soret effect, giving rise to both absolute and convective instability.

DOI: 10.1103/PhysRevE.75.066206 PACS number(s): 05.45.−a, 66.10.Cb, 82.40.Ck

I. INTRODUCTION

A temperature gradient across a fluid mixture not only causes a heat flux, but also gives rise to a diffusion current of the constituent components. This net mass flux induces the buildup of a concentration gradient parallel or antiparallel to the thermal gradient. This thermal diffusion, known as the Ludwig-Soret effect, is a cross effect between temperature and concentration, whose existence was for the first time observed in 1856 by Ludwig and then independently established by Soret in 1879 [1–3]. Signatures of this effect can be widely seen in thermohaline convection in oceans and component segregation in liquid lava, and it has also been used for the purification of isotopes, polymer characterization, and separation of metals from alloys [4–6]. The Soret effect has been explicitly studied recently in many systems, ranging from simple binary fluid mixtures to complex molecular systems such as soluted surfactants, colloidal suspensions, and charged micelles [7–10]. Along with the phenomenological and microscopic description of the effect, accurate measurements of the thermal diffusion ratios have been made by several groups, by employing various optical techniques like beam deflection and Rayleigh scattering, and also by thermogravitational column methods and thermal field flow fractionation [7,11,12].

In this paper, we consider the Soret effect in a reactive system where the components undergoing chemical reaction are ionic in nature. Considering that a thermal gradient will also have an impact on the migration and transport of the ions, one may envisage that thermal diffusion may act as a thermodynamic cross effect in a reaction-diffusion system. The interaction between this diffusion and the nonlinearity involved in chemical kinetics of the reacting components is likely to bring about spatiotemporal instability, leading to stationary pattern formation or wave propagation in a spatially extended system, when the latter is driven out of equilibrium. Although the Soret effect in reactive, homogeneous systems has been observed [8], and modification by an electromagnetic field of the fluxes of the ionic components of reaction-diffusion systems, leading to stoppage, annihilation, and aggravation of chemical waves and stationary patterns [13–15] and the loss of symmetry of traveling wave fronts under the influence of cubic autocatalytic kinetics [16] are well known, the effect of thermodiffusion in inducing instability in reaction-diffusion systems has largely remained unexplored. Our object in this paper is to study a planar ionic reaction-diffusion system driven by a constant thermal gradient, and to look for the onset of thermal-diffusion-induced instabilities. As a prototypical example, we have considered the arsenous acid–iodate system, which has been a good testing ground for various features of nonlinear chemical dynamics over the years [17,18]. In what follows we show that thermodiffusion may bring about spatiotemporal instability in this system and, depending on the appropriate parameter region and Soret coefficient, it is possible to realize the convective and absolute instability regimes and chemical wave propagation. We corroborate our theoretical analysis by numerical simulations in two dimensions.

II. THERMODIFFUSION IN A REACTION-DIFFUSION SYSTEM: THE MODEL

We have chosen as our model one of the simplest chemical systems that has been widely used by several groups for the study of wave-front propagation and noise-induced instability, the arsenous acid–iodate reaction. Detailed studies made by Showalter and co-workers [19] have portrayed the varied wave-front characteristics of this reaction. Different experimental and numerical works analyzing the dependence of the wave-front velocity on the stoichiometry and the ratio of the diffusivities of autocatalyst and reactants in this system have been carried out [20,21].

The arsenous acid–iodate system is a composite of two reactions, viz., the Dushman reaction (2.1) and the Roebuck reaction (2.2), which have been known for over a century:

$$IO_3^- + 5I^- + 6H^+ \leftrightharpoons 3I_2 + 3H_2O, \tag{2.1}$$

$$H_3AsO_3 + I_2 + H_2O \rightarrow H_3AsO_4 + 2I^- + 2H^+. \tag{2.2}$$

In the overall process, the Dushman reaction is the rate-determining step [19,22]. We have here followed the kinetic studies of the latter as given by Schmitz [23], where the experimental observation of the simultaneous first- and second-order dependence of the rate on $[I^-]$ over a range of low to moderately low concentration of I^- has been made. The elementary steps involved in the mechanism of the Dushman reaction as suggested by Schmitz are as follows:

$$IO_3^- + H^+ \leftrightharpoons HIO_3, \tag{2.3}$$

*Electronic address: pcdsr@mahendra.iacs.res.in

$$HIO_3 + I^- + H^+ \leftrightharpoons I_2O_2 + H_2O, \tag{2.4}$$

$$I_2O_2 + H_2O \rightarrow HIO_2 + HOI, \tag{2.5}$$

$$I_2O_2 + I^- \rightarrow IO_2^- + I_2. \tag{2.6}$$

The experimental rate law for the system is given by

$$\frac{d[I^-]}{dt} = (k_1 + k_2[I^-])[I^-][IO_3^-][H^+]^2, \tag{2.7}$$

where $k_1 = 4.5 \times 10^3 M^{-3}\ s^{-1}$ and $k_2 = 1.0 \times 10^8 M^{-4}\ s^{-1}$ are the rate constants. Here M stands for mol dm^{-3}, the unit of molar concentration.

The conspicuous feature of this reaction is the role of I_2 as an intermediate. The sharp change in concentration of the iodine-containing species, viz., I^-, IO_3^-, and I_2, as functions of time in a stirred batch reactor is another interesting characteristic of this reaction. This allows the assumption that all the iodine is present as either I^- or IO_3^-, the concentration of I_2 being negligible as compared to these two species [24].

The present study begins with a note that, when the system is spatially extended, a sharp change in concentration of iodine-containing species with time is likely to make the spatial local gradient of these species appreciably sharp.

In view of these discussions, we have the following rate equations for the three ionic species $[I^-]$, $[IO_3^-]$, and $[H^+]$, respectively (details of the kinetics are included in the Appendix):

$$\frac{d[I^-]}{dt} = (k_1 + k_2[I^-])[I^-][IO_3^-][H^+]^2 - \nabla \cdot J_{[I^-]}, \tag{2.8}$$

$$\frac{d[IO_3^-]}{dt} = -\nabla \cdot J_{[IO_3^-]}, \tag{2.9}$$

$$\frac{d[H^+]}{dt} = -\nabla \cdot J_{[H^+]}, \tag{2.10}$$

where J_i denotes the flux of the ith ionic species for the system.

For a reaction-diffusion system in the presence of a thermal gradient, the flux for an ionic species is given by the Ludwig-Soret effect as

$$J_i = -D_i \nabla C_i - D_{T_i} C_i (1 - c_i) \nabla T, \tag{2.11}$$

where D_i denotes the translational diffusion coefficient, D_{T_i} is the thermal diffusion coefficient, C_i is the molar concentration of the ith ion, c_i is the relative concentration of the same (i.e., $c_i = C_i / \Sigma C_i$), and ∇T is the thermal gradient between two sides of the reaction vessel and a constant. D_{T_i} can be expressed in the form

$$D_{T_i} = S_{T_i} D_i, \tag{2.12}$$

S_{T_i} being the Soret coefficient of the ith ionic species which is given as [8]

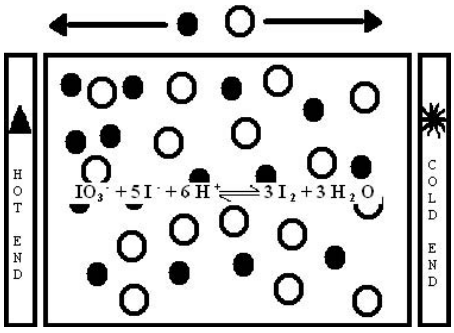

FIG. 1. Schematic diagram of an ionic reaction under the influence of a constant thermal gradient, where the different components, light and heavy, move to different ends of the reaction vessel, depicting thermodiffusion.

$$S_{T_i}^{-1} = S_{T_0}^{-1}(1 + k_s C_i), \tag{2.13}$$

k_s being a phenomenological constant. The values of S_{T_0} for ionic species being nearly equal, we omit the subscript i for the same.

Thus, Eq. (2.11) takes the form

$$J_i = -D_i \nabla C_i - D_i S_{T_0} C_i \frac{(1 - C_i c_T)}{(1 + k_s C_i)} \nabla T, \tag{2.14}$$

where $c_T = 1/\Sigma C_i$.

On substituting the expression for the flux, Eq. (2.8) takes the form

$$\frac{d[I^-]}{dt} = (k_1 + k_2[I^-])[I^-][IO_3^-][H^+]^2 + D_{[I^-]} \nabla \cdot \left(\nabla[I^-] + S_{T_0}[I^-] \frac{(1 - [I^-]c_T)}{(1 + k_s[I^-])} \nabla T \right). \tag{2.15}$$

Now we substitute $u(x,y,t)$, $v(x,y,t)$, and $w(x,y,t)$ for $[I^-]$, $[IO_3^-]$, and $[H^+]$, respectively. Considering $D_{I^-} = D_{IO_3^-} = D_{H^+}/d = 1$, we obtain the following forms of the rate equations in a similar way:

$$\frac{\delta u(x,y,t)}{\delta t} = (k_1 + k_2 u) u v w^2 + \nabla \left(\nabla u + S_{T_0} \frac{u(1 - u c_T)}{(1 + k_s u)} \nabla T \right), \tag{2.16}$$

$$\frac{\delta v(x,y,t)}{\delta t} = \nabla \left(\nabla v + S_{T_0} \frac{v(1 - v c_T)}{(1 + k_s v)} \nabla T \right), \tag{2.17}$$

$$\frac{\delta w(x,y,t)}{\delta t} = d \nabla \left(\nabla w + S_{T_0} \frac{w(1 - w c_T)}{(1 + k_s w)} \nabla T \right). \tag{2.18}$$

A schematic diagram of the movement of ions under the influence of thermodiffusion has been depicted in Fig. 1. The components in a mixture move to different ends of the Soret cell as per the sign of their Soret coefficients. Those with positive coefficient move to the colder region and ones with negative Soret coefficient move toward the hot end. An explanation of this phenomenon given by Prigogine *et al.* was that the sign of S_{T_0} is determined by the difference of the

cohesion densities (energy of vaporization divided by molar volume) of the pure constituents of a binary liquid mixture [25]. The constituent with higher density of cohesion is enriched at the cold wall. Other views on the change of sign of the Soret coefficient are also found, based on the concepts of heat of transport [26] and the temperature and concentration dependence of the Soret coefficient [27].

III. CONVECTIVE AND ABSOLUTE INSTABILITIES

We assume the existence of a spatially uniform steady state $(u=u_0,v=v_0,w=w_0)$ of the dynamical system, such that

$$f(u_0,v_0,w_0)=0, \tag{3.1}$$

where $f(u,v,w)$ denotes the kinetic part of Eq. (2.10). We furthermore assume that this state is stable in the absence of diffusion, i.e.,

$$\left[\frac{\delta f}{\delta u}\right]_{u=u_0,v=v_0,w=w_0}=f'<0. \tag{3.2}$$

The stability of the steady state as implied in Eq. (3.2) is purely kinetic in nature. Since we are interested in the stable homogeneous steady state, it is also necessary to ensure that the choice of parameter space does not lead to instability when the diffusion ratio is incorporated in the analysis. Considering an expansion of u, v, and w in Eq. (2.16) about the steady value (u_0,v_0,w_0), and keeping only the linear terms in $\delta\bar{u}$, $\delta\bar{v}$, $\delta\bar{w}$, we have

$$\begin{aligned}\frac{\delta(\delta\bar{u})}{\delta t}&=v_0w_0^2k_1\delta\bar{u}+u_0w_0^2k_1\delta\bar{v}+2u_0v_0w_0k_1\delta\bar{w}\\&+2u_0v_0w_0^2k_2\delta\bar{u}+u_0^2w_0^2k_2\delta\bar{v}+2u_0^2v_0w_0k_2\delta\bar{w}+\nabla_{x,y}^2\delta\bar{u}\\&+S_{T_0}\nabla T\left[\frac{1-u_0c_T}{(1+k_su_0)^2}-\frac{u_0c_T}{(1+k_su_0)}\right]\nabla_{x,y}\delta\bar{u},\end{aligned} \tag{3.3}$$

where the terms within the square brackets correspond to the first derivative of the Soret term at the point (u_0,v_0,w_0), or $(\delta/\delta u)[u(1-uc_T)/(1+k_su)]_{u=u_0,v=v_0,w=w_0}$.

Proceeding similarly, Eqs. (2.17) and (2.18) take the forms

$$\frac{\delta(\delta\bar{v})}{\delta t}=\nabla_{x,y}^2\delta\bar{v}+S_{T_0}\nabla T\left[\frac{1-v_0c_T}{(1+k_sv_0)^2}-\frac{v_0c_T}{(1+k_sv_0)}\right]\nabla_{x,y}\delta\bar{v}, \tag{3.4}$$

$$\begin{aligned}\frac{\delta(\delta\bar{w})}{\delta t}&=d\nabla_{x,y}^2\delta\bar{w}+dS_{T_0}\nabla T\left[\frac{1-w_0c_T}{(1+k_sw_0)^2}\right.\\&\left.-\frac{w_0c_T}{(1+k_sw_0)}\right]\nabla_{x,y}\delta\bar{w}.\end{aligned} \tag{3.5}$$

We now express the spatiotemporal perturbations as

$$\delta\bar{u}(x,y,t)=Ae^{i(k_x\cdot x+k_y\cdot y-\omega t)}, \tag{3.6}$$

$$\delta\bar{v}(x,y,t)=Be^{i(k_x\cdot x+k_y\cdot y-\omega t)}, \tag{3.7}$$

$$\delta\bar{w}(x,y,t)=Ce^{i(k_x\cdot x+k_y\cdot y-\omega t)}, \tag{3.8}$$

where A, B, and C are constants. Substituting the above into Eqs. (3.3)–(3.5), we have

$$\begin{aligned}-i\omega A&=(v_0w_0^2k_1+2u_0v_0w_0^2k_2)A+(u_0w_0^2k_1+u_0^2w_0^2k_2)B\\&+2(u_0v_0w_0k_1+u_0^2v_0w_0k_2)C-(k_x+k_y)^2A+i(k_x\\&+k_y)S_{T_0}\nabla T\left(\frac{1-u_0c_T}{(1+k_su_0)^2}-\frac{u_0c_T}{(1+k_su_0)}\right)A,\end{aligned} \tag{3.9}$$

$$\begin{aligned}-i\omega B&=-(k_x+k_y)^2B+i(k_x+k_y)S_{T_0}\nabla T\left(\frac{1-v_0c_T}{(1+k_sv_0)^2}\right.\\&\left.-\frac{v_0c_T}{(1+k_sv_0)}\right)B,\end{aligned} \tag{3.10}$$

$$\begin{aligned}-i\omega C&=-d(k_x+k_y)^2C+i(k_x+k_y)dS_{T_0}\nabla T\left(\frac{1-w_0c_T}{(1+k_sw_0)^2}\right.\\&\left.-\frac{w_0c_T}{(1+k_sw_0)}\right)C.\end{aligned} \tag{3.11}$$

The system of equations (3.9)–(3.11) can be put in the form of a matrix equation as [from now onwards we replace (k_x+k_y) by k]

$$L\begin{pmatrix}A\\B\\C\end{pmatrix}=0, \tag{3.12}$$

where

$$L=\begin{pmatrix}l_{11}+i\omega & l_{12} & l_{13}\\0 & l_{22}+i\omega & 0\\0 & 0 & l_{33}+i\omega\end{pmatrix}.$$

Here the expressions for the nonzero elements of the above matrix are as follows:

$$\begin{aligned}l_{11}&=[(v_0w_0^2k_1+2u_0v_0w_0^2k_2)-k^2]+ikS_{T_0}\nabla T\left(\frac{1-u_0c_T}{(1+k_su_0)^2}\right.\\&\left.-\frac{u_0c_T}{(1+k_su_0)}\right),\end{aligned} \tag{3.13}$$

$$l_{12}=(u_0w_0^2k_1+u_0^2w_0^2k_2), \tag{3.14}$$

$$l_{13}=(2u_0v_0w_0k_1+2u_0^2v_0w_0k_2), \tag{3.15}$$

$$l_{22}=-k^2+ikS_{T_0}\nabla T\left(\frac{1-v_0c_T}{(1+k_sv_0)^2}-\frac{v_0c_T}{(1+k_sv_0)}\right), \tag{3.16}$$

$$l_{33}=-dk^2+ikdS_{T_0}\nabla T\left(\frac{1-w_0c_T}{(1+k_sw_0)^2}-\frac{w_0c_T}{(1+k_sw_0)}\right). \tag{3.17}$$

For the sake of simplicity the constant term $(v_0w_0^2k_1+2u_0v_0w_0^2k_2)$ will henceforth be replaced by a_0. In the same

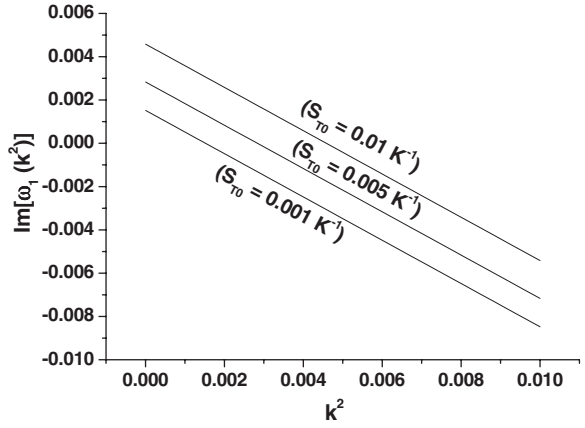

FIG. 2. Dispersion relation [Im(ω) versus k^2] for varying S_{T_0}, fixed ∇T (=0.5 K), fixed k_s (=7×10^4 mol^{-1} dm^3), and other parameters as mentioned in the text.

spirit we also incorporate the following abbreviations:

$$M_1 = \left(\frac{1-u_0c_T}{(1+k_su_0)^2} - \frac{u_0c_T}{(1+k_su_0)}\right),$$

$$M_2 = \left(\frac{1-v_0c_T}{(1+k_sv_0)^2} - \frac{v_0c_T}{(1+k_sv_0)}\right),$$

$$M_3 = \left(\frac{1-w_0c_T}{(1+k_sw_0)^2} - \frac{w_0c_T}{(1+k_sw_0)}\right).$$

To examine the stability, we now write the following determinantal equation for the eigenvalue problem:

$$|L| = 0. \tag{3.18}$$

On expanding Eq. (3.18), we get the following dispersion relations:

$$\omega_1 = i(a_0 - k^2) - kS_{T_0}\nabla TM_1, \tag{3.19}$$

$$\omega_2 = -ik^2 - kS_{T_0}\nabla TM_2, \tag{3.20}$$

$$\omega_3 = -ik^2 - kS_{T_0}\nabla TM_3. \tag{3.21}$$

Spatial instability sets in as Im[$\omega(k^2)$] attains a positive value. We now look for the range of k^2 values for which the imaginary parts of the eigenvalues $\omega(k^2)$ attain a positive value for a given constant temperature gradient ∇T and a particular value of the Soret coefficient S_{T_0}.

The experimentally admissible parameters [24] are given by $k_1=4.5\times10^3M^{-3}$ s^{-1}, $k_2=1.0\times10^8M^{-4}$ s^{-1}, and $D_{H^+}=2\times10^{-1}$ mm^2 s^{-1} (giving $d=2$); and the initial conditions used are $u_0=6.0\times10^{-3}M$; $v_0=0.0M$; $w_0=7.1\times10^{-3}M$. Figure 2 depicts the range of the k^2 values for some constant thermal gradient (∇T=0.5 K), a fixed value of k_s (=7×10^4 M^{-1}), and several values of S_{T_0} (=1.3×10^{-4}–1.0×10^{-2} K^{-1}) for which a small perturbation may bring about an instability with time.

Following Scott *et al.* [28], we now distinguish between three typical situations: absolute instability, convective instability, and stationary pattern formation.

A. Absolute instability

When a small perturbation lifts the system to a state different from the initial, and the perturbation moves forward, transforming the system to a final state away from the steady state, the system is said to be absolutely unstable. The present context, when both the real as well as the imaginary parts of the eigenvalues are nonzero, implies absolute instability. The presence of the real part in the solution of the eigenvalues, Re(ω), signifies a nonzero imaginary time part in the exponential part of the spatiotemporal perturbations, $e^{-i\omega t}$ [Eq. (3.6)], and thus predicts wave front propagation in a system with no back. On the other hand, the imaginary part of the eigenvalues Im(ω), i.e., the real time part in the exponential of the perturbation, promises a final state that is different from the initial state. We will return to the specific nature of the wave front propagation under the influence of absolute instability as depicted in Fig. 5(a) in the next section, viz., numerical simulation.

B. Convective instability

A spatially extended system is said to be convectively unstable if a perturbation induces a local growth away from the spatially uniform steady state, and the disturbance then propagates as a wave packet growing in size. But, unlike in the case of absolute instability, in this case, when the wave packet passes by, the system comes back to the original steady state. The condition of convective instability is given by the reality of the eigenvalues ω; i.e., Im[$\omega(k_0)$]=0. In what follows we will again discuss the propagation of the wave front with time, when the system is convectively unstable, in Sec. IV, as portrayed in Fig. 5(b).

C. Stationary pattern

When the perturbation is constant with time, with a purely imaginary exponent, it can give rise to a stationary pattern, i.e., the exponential part should be of the form $e^{i(k_xx+k_yy)}$, such that $\omega=0$ and k_x and k_y are real.

In order to find the appropriate condition for the transition between absolute and convective instability, we proceed as follows. From Eq. (3.19) one obtains

$$\frac{\delta\omega}{\delta k} = -2ik - S_{T_0}\nabla TM_1. \tag{3.22}$$

We find the maximum at k_0 such that $[\delta\omega/\delta k]_{k=k_0}=0$, which yields,

$$k_0 = \frac{i}{2}S_{T_0}\nabla TM_1. \tag{3.23}$$

Therefore, Eq. (3.19) takes the form

$$\omega(k_0) = ia_0 - \frac{i}{4}(S_{T_0}\nabla T)^2M_1^2. \tag{3.24}$$

The region of parameter space where Im[$\omega(k_0)$]=0 foretells the onset of convective instability. In this space we have

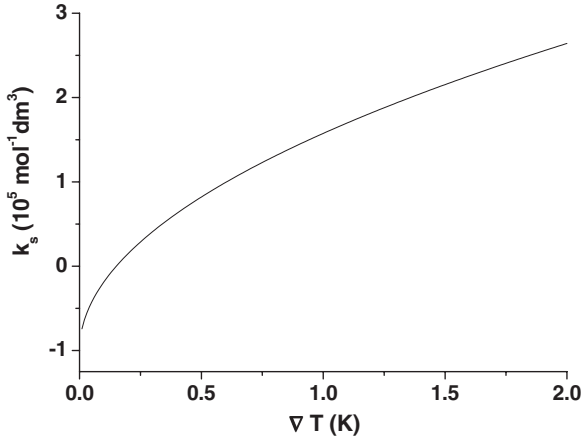

FIG. 3. Plot of k_s with varying temperature gradient ∇T for a fixed value of S_{T_0} (=6.5×10^{-3} K^{-1}) and other parameters as mentioned in the text.

$$M_1^2 = \frac{4a_0}{(S_{T_0}\nabla T)^2} = N^2 \tag{3.25}$$

where N^2 is an abbreviation incorporated for simplicity.

An expression for k_s can be obtained from M_1 as defined earlier,

$$k_s = \frac{1}{u_0}\left(-1 + \frac{[-u_0 \pm \sqrt{u_0^2 - 4N(u_0-1)}]}{2N}\right). \tag{3.26}$$

On the other hand, Eq. (3.25) gives us an expression for S_{T_0} as

$$S_{T_0} = \frac{\sqrt{4a_0}}{\nabla T M_1}. \tag{3.27}$$

A look at the variation of k_s keeping the Soret coefficient constant, and vice versa, with changing values of ∇T gives us an idea of the role of the thermal gradient in bringing about characteristic changes in the diffusion of components of a reaction mixture. Figures 3 and 4 portray the plots of k_s and S_{T_0}, respectively, with varying ∇T. The region of space below the curve in Fig. 4 depicts the region of absolute instability and that above it stands for a convectively unstable state. The range of the Soret coefficient values matches well with the experimental results for electrolytes, where Soret coefficients are of the order of $\approx10^{-3}$ K^{-1} [29,30]. Whereas, in polymeric solutions $S_{T_0}\approx0.5$ K^{-1}. Recently, values of S_{T_0} from 0.25 *to* 0.17 K^{-1} have been reported in magnetic colloidal systems [9].

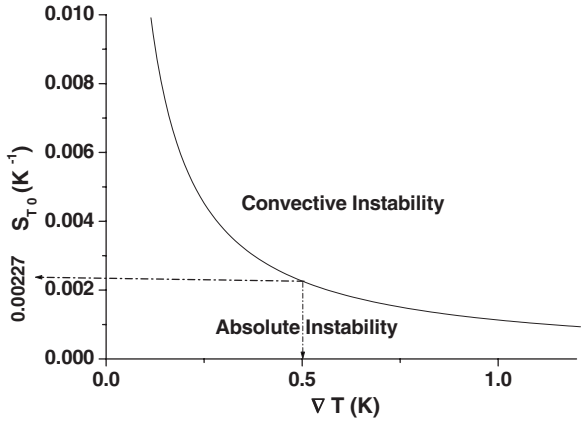

FIG. 4. Variation of S_{T_0} with changing temperature gradient ∇T, the plot depicting the transition from absolute to convective instability. Here $k_s=7\times10^4$ mol^{-1} dm^3) and other parameters are as mentioned in the text.

The condition for transition to stationary patterns can be found by imposing $\omega=0$, so that the perturbation has the form $e^{i(k_x x+k_y y)}$. From Eq. (3.18), we then have

$$k^5 S_{T_0}\nabla T(M_1+M_2+M_3)d - k^3 S_{T_0}\nabla T[(M_2+M_3)a_0 + (S_{T_0})^2(\nabla T)^2 M_1M_2M_3]d = 0. \tag{3.28}$$

This gives us an expression for k as

$$k = \left(\frac{(S_{T_0})^2(\nabla T)^2 M_1M_2M_3 + (M_2+M_3)a_0}{M_1+M_2+M_3}\right)^{1/2}. \tag{3.29}$$

Expressing Eq. (3.28) in terms of the variation of S_{T_0} versus ∇T, we have

$$\begin{aligned}[(S_{T_0})^2(\nabla T)^2]^2&\left(\frac{(M_1M_2M_3)^2}{(M_1+M_2+M_3)^2}a_0 - \frac{M_1M_2M_3(M_1M_2+2M_2M_3)}{M_1+M_2+M_3}\right)\\ &+ (S_{T_0})^2(\nabla T)^2\left(\frac{(M_2+M_3)(M_1M_2M_3)}{(M_1+M_2+M_3)^2}a_0 - \frac{(M_2+M_3)(M_1M_2+2M_2M_3)}{M_1+M_2+M_3} - M_2M_3a_0\right)\\ &+ \frac{(M_2+M_3)^2}{(M_1+M_2+M_3)^2}a_0^3 = 0.\end{aligned} \tag{3.30}$$

A deeper look into Eq. (3.30) reveals that, under the imposed conditions, there exists no such locus in real parameter space that may indicate the existence of stationary patterns. This predicts that, in the arsenous acid–iodate system, thermal diffusion is not expected to lead to the onset of patterns stationary in time.

IV. NUMERICAL SIMULATIONS AND DISCUSSION

A. Numerical simulation: Wave propagation

In order to explore our stability analysis further, we now carry out numerical simulations of the reaction-diffusion system [Eqs. (2.16)–(2.18)], using the explicit Euler method for the integration of the equations, following discretization of space and time. A finite system size of 100×100 grid points has been chosen. Zero-flux boundary conditions have been considered along all the four walls. A time interval Δt =0.000 01 s and a cell size Δx=0.1 mm have been found to be appropriate for the purpose.

We have carried out our numerical simulations for

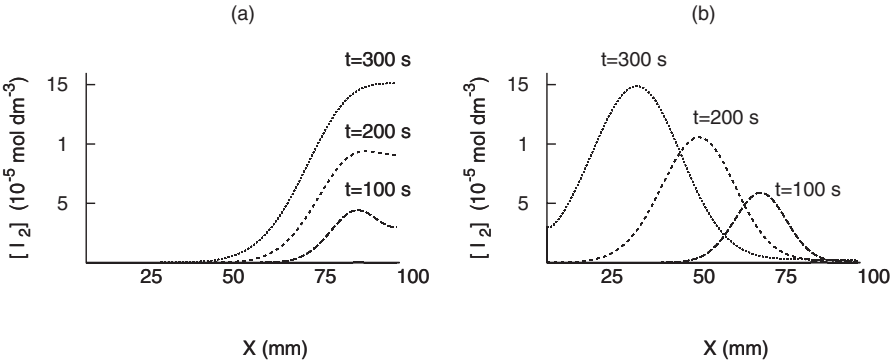

FIG. 5. Concentration of iodine versus the direction of wave propagation at different times, depicting the influence of (a) absolute instability and (b) convective instability.

different values of S_{T_0}, ranging from -1.3×10^{-4} to 6.5×10^{-2} K^{-1}. We impose a constant thermal gradient ($\nabla T=0.5$ K) and a fixed value of k_s ($=7\times10^4$ M^{-1}). The initial conditions are taken identical to the initial experimental values of the reactants, with $u_0=1.0\times10^{-6}M$, $v_0=0.006M$, over the unreacted reaction surface ahead of the front. The small area behind the front is considered as that where the reaction has already taken place, and the initial value of the iodide ion concentration here is considered to be $u_0=0.006M$, and that of the iodate $v_0=1.0\times10^{-6}M$. The hydrogen ion, or acid catalyst, which acts as a buffer, is taken to be initially uniform all over the reaction vessel with a concentration of $w_0=0.0071M$. The rate constants k_1 and k_2 are the experimentally admissible values mentioned earlier.

We calculate the iodine concentration at any time t, as a function of the concentrations of iodide and iodate ions, taking into consideration the conservation of total iodine in the system:

$$[I_2]_t=\frac{1}{2}([I^-]_0+[IO_3]_0-[I^-]_t+[IO_3^-]_t). \qquad (4.1)$$

Figure 5 represents the wave front as a plot of the iodine concentration versus the direction of wave propagation, at three different times. In Figs. 6–10, we show the surface plots of the iodine concentration, changing with time. As the wave packet moves forward it forms a concentration gradient of the reactants, as shown in the figures. The reactant concentration behind the wave front may increase to a constant value as seen in the case of low S_{T_0}($=1.3\times10^{-4}$ and 1.3×10^{-3} K^{-1}) values (Figs. 6 and 7). This situation closely resembles the state of absolute instability. It matches with the case in Fig. 5(a), where the maximum of the wave front increases with no back.

For still higher values of the Soret coefficient ($S_{T_0}\geqslant2.27\times10^{-3}$ K^{-1}), the wave front moves forward as a maximum, and the concentration behind the wave front starts to decrease with time. This is displayed by the surface plot of iodine concentration (Fig. 8). The trend is clearer for higher values of S_{T_0} ($=3.9\times10^{-2}$ and 6.5×10^{-2} K^{-1}) as is evident from Figs. 9 and 10. This type of wave propagation is indicative of convective instability. The plot in Fig. 5(b) signifies the specific nature of the wave under this kind of instability.

In keeping with our analysis, a further variation of S_{T_0} to either higher or lower values does not lead to the formation of stationary patterns.

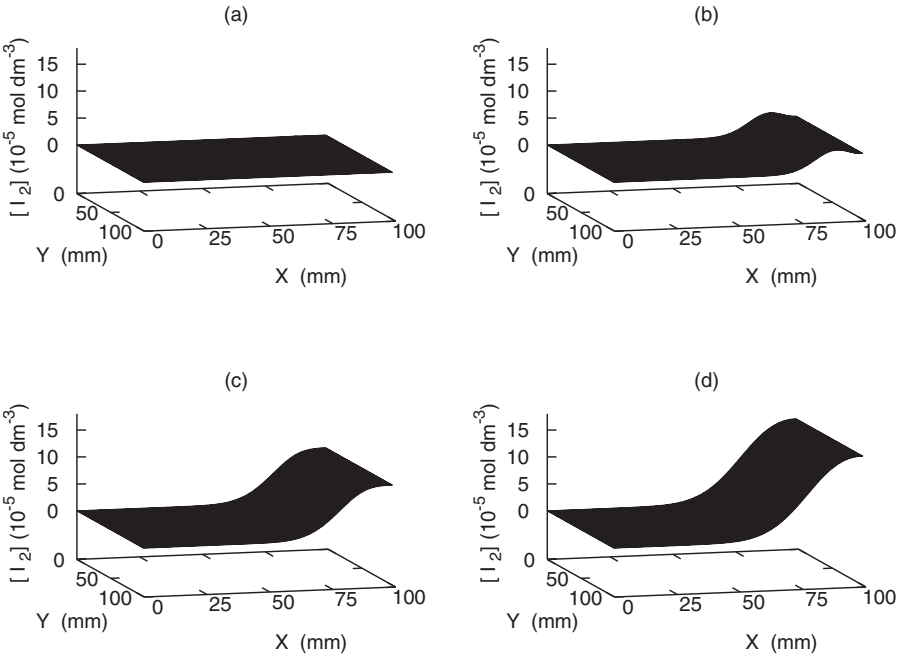

FIG. 6. Time-evolved surface plots of the concentration of iodine for Soret coefficient value of $S_{T_0}=1.3\times10^{-4}$ K^{-1}, showing absolute instability: (a) 10, (b) 100, (c) 200, and (d) 300 s. (Other parameters are as mentioned in the text.)

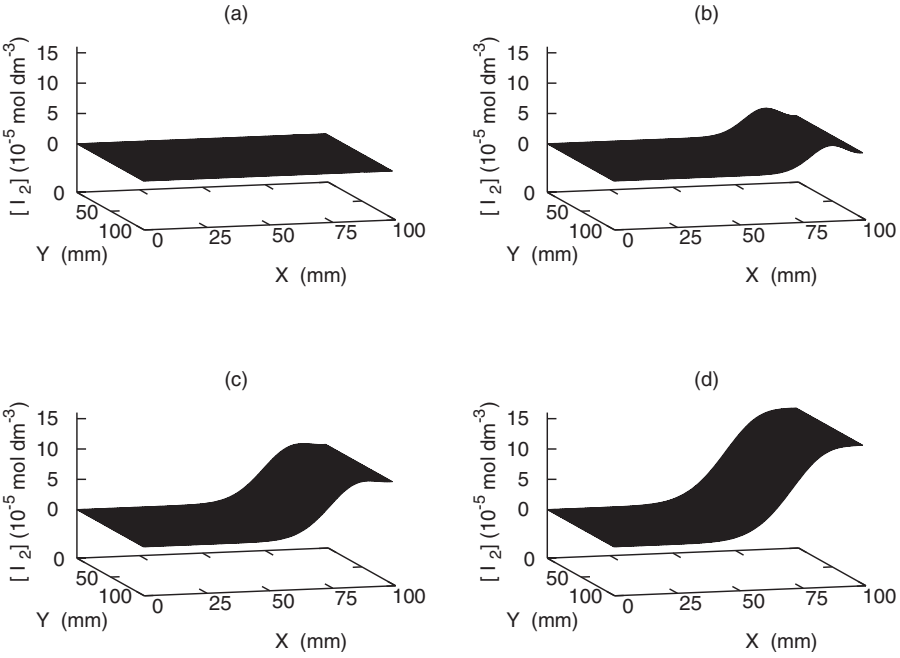

FIG. 7. Time-evolved surface plots of the concentration of iodine for Soret coefficient value of $S_{T_0}=1.3\times10^{-3}$ K^{-1} showing absolute instability: (a) 10, (b) 100, (c) 200, and (d) 300 s. (Other parameters are as mentioned in the text.)

We also observe the time (t_m) required by the maximum of the propagating wave front to reach a particular point. The initial conditions has been set as in the previous case. It is seen from a plot of t_m vs S_{T_0} (Fig. 11), that t_m varies hyperbolically with respect to S_{T_0}, with asymptotes at $x=0$ and $y=0$. There can be seen a distinct break in the curve, which occurs due to the shift between absolute and convective instabilities. The region around which this transition occurs ($S_{T_0}=2.27\times10^{-3}$ K^{-1}, $\nabla T=0.5$ K) is in coherence with the analytical result (Fig. 4).

B. Possible experimental setup

Keeping in view recent developments, it is apparent that theoretical studies of such instability-inducing effects of thermodiffusion on reaction-diffusion systems have not yet been performed. As has been predicted by both our analysis and numerical simulations, a slight variation in the value of the Soret coefficient can cause a crossover between the absolute and convective instabilities, thus bringing about appreciable changes in the wave front properties. The high sensitivity of the arsenous acid–iodate reaction, which establishes it as one of the best systems for the study of wave front propagation [17,22,24], also ensures the monitoring of this effect of thermodiffusion, within workable ranges of experimental constants. For the investigation of the spatiotemporal dynamics in our system, we can carry out our experiment in an acrylamide gel phase in the presence of starch as an indicator [20]. The resulting gel can then be placed on a Peltier ele-

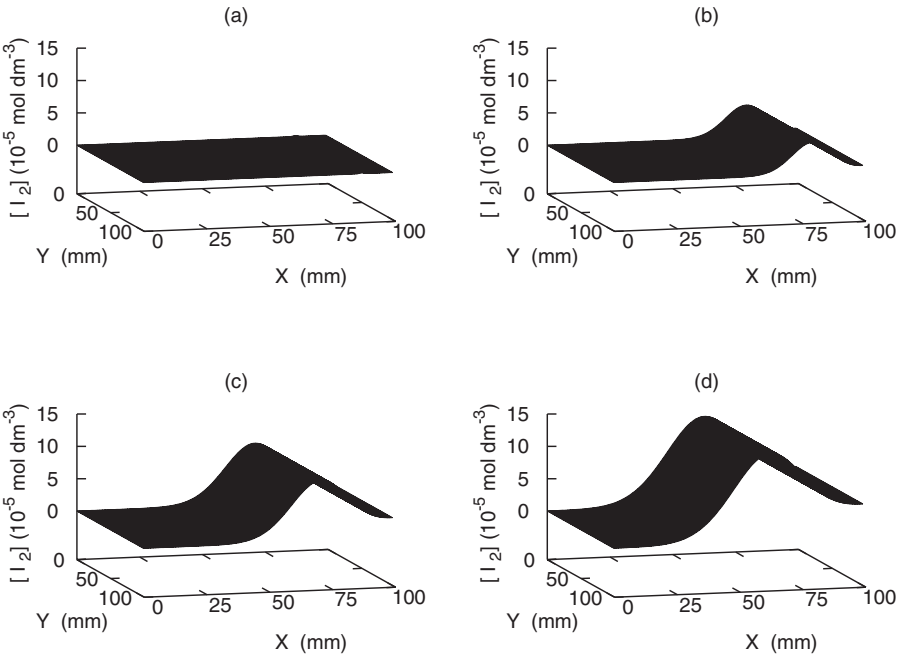

FIG. 8. Time-evolved surface plots of the concentration of iodine for Soret coefficient value of $S_{T_0}=2.34\times10^{-3}$ K^{-1} showing the advent of convective instability: (a) 10, (b) 100, (c) 200, and (d) 300 s. (Other parameters are as mentioned in the text.)

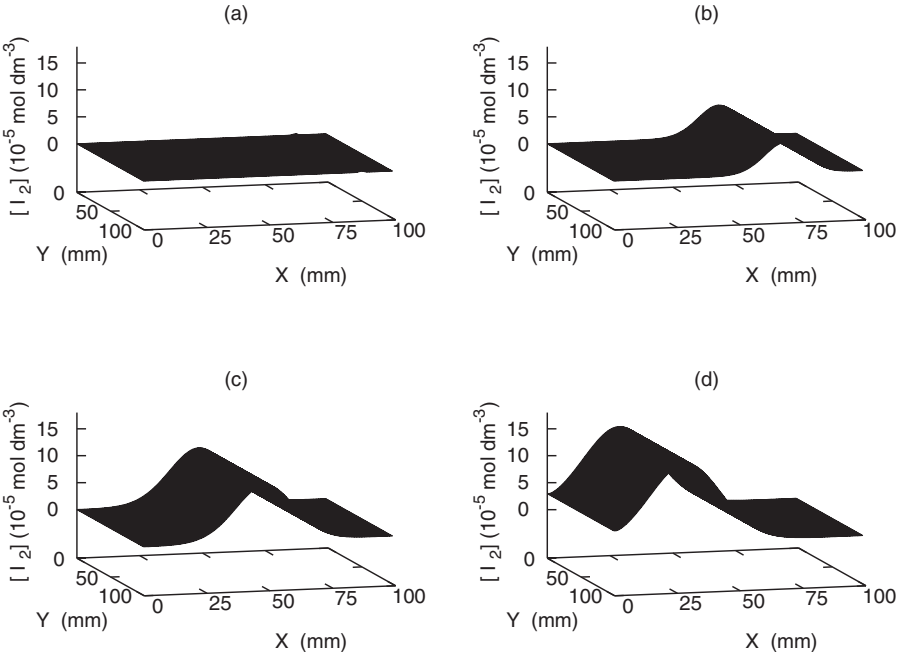

FIG. 9. Time-evolved surface plots of the concentration of iodine for Soret coefficient value of $S_{T_0}=3.9\times10^{-2}$ K^{-1} showing convective instability: (a) 10, (b) 100, (c) 200, and (d) 300 s. (Other parameters are as mentioned in the text.)

ment, which can control the temperature, in order to produce spatial temperature gradients in the gel. The current flow through this element can be controlled by a computer so as to cool one-half of the element while heating the other end, thus establishing a well-defined temperature gradient. The temperature of the gel can be measured by a thermocouple, and the wave front propagation measured by a camera and other necessary devices. Such experimental setups have been employed in recent studies of biochemical oscillatory systems [31].

V. CONCLUSION

In this paper, we have studied the effect of a thermal gradient on an ionic reaction-diffusion system, the iodate–arsenous acid reaction. It has been shown that thermal diffusion, which appears as a thermodynamic cross effect between concentration flux and thermal gradient, results in convection terms, thus giving rise to absolute and convective instabilities, in the presence of a chemical reaction. The thermodiffusion-induced instabilities are appropriate for wave propagation of different types. We also suggest a probable experimental setup to study our model. We hope this approach will be useful for exploring the role of the Soret effect in initiating instability in other chemical systems and in the modeling of flow-distributed oscillations.

ACKNOWLEDGMENT

Thanks are due to the Council of Scientific and Industrial Research, Government of India, for support (S.D.).

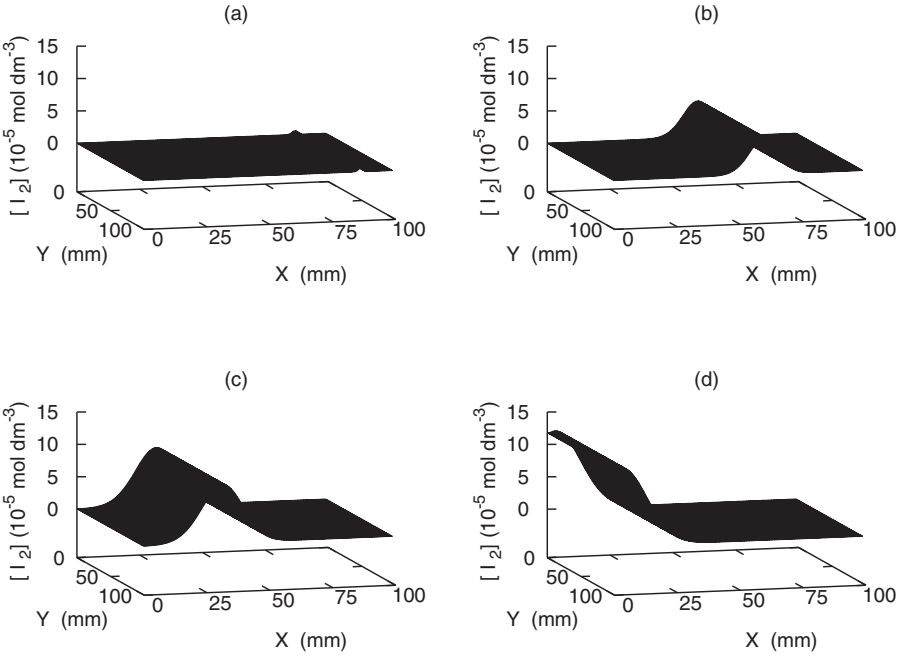

FIG. 10. Time-evolved surface plots of the concentration of iodine for Soret coefficient value of $S_{T_0}=6.5\times10^{-2}$ K^{-1} showing convective instability: (a) 10, (b) 100, (c) 200, and (d) 300 s. (Other parameters are as mentioned in the text.)

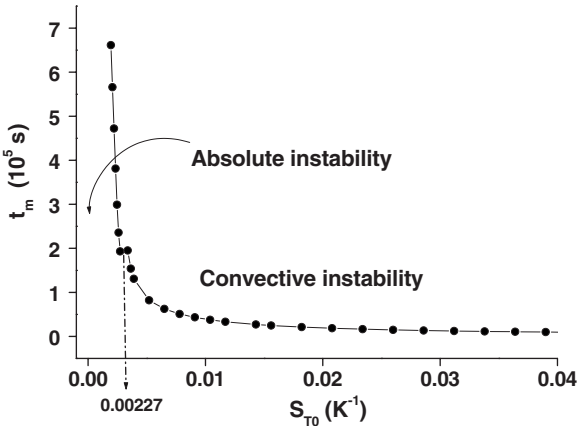

FIG. 11. Plot of t_m versus S_{T_0} for the parameter range mentioned in the text.

APPENDIX

The rate laws of the different species involved in the elementary steps of the Dushman reaction are as follows:

$$\frac{d[IO_3^-]}{dt} = -k_3[IO_3^-][H^+] + k_{-3}[HIO_3], \tag{A1}$$

$$\frac{d[H^+]}{dt} = -k_3[IO_3^-][H^+] + k_{-3}[HIO_3] - k_4[HIO_3][I^-][H^+] + k_{-4}[I_2O_2][H_2O], \tag{A2}$$

$$\frac{d[HIO_3]}{dt} = k_3[IO_3^-][H^+] - k_{-3}[HIO_3] - k_4[HIO_3][I^-][H^+] + k_{-4}[I_2O_2][H_2O], \tag{A3}$$

$$\frac{d[I_2O_2]}{dt} = k_4[HIO_3][I^-][H^+] - k_{-4}[I_2O_2][H_2O] - k_5[I_2O_2] \times [H_2O] - k_6[I_2O_2][I^-], \tag{A4}$$

$$\frac{d[I^-]}{dt} = -k_4[HIO_3][I^-][H^+] - k_6[I_2O_2][I^-], \tag{A5}$$

$$\frac{d[I_2]}{dt} = k_6[I_2O_2][I^-]. \tag{A6}$$

Applying steady state approximations to HIO_3 and I_2O_2 and considering $[H^+]$ constant (due to the large concentration of H^+ ions), we arrive at the following rate equation:

$$\frac{d[I^-]}{dt} = [IO_3^-][I^-][H^+]^2(k' + k''[I^-]), \tag{A7}$$

where k' and k'' are constants, in keeping with the experimental rate law.

Also this implies that

$$\frac{d[IO_3^-]}{dt} = 0, \tag{A8}$$

$$\frac{d[H^+]}{dt} = 0. \tag{A9}$$

[1] C. Ludwig, Sitzungsber. Akad. Wiss. Wien, Math.—Naturwiss. Kl. Z **20**, 539 (1856).
[2] C. Soret, Arch. Sci. Phys. Nat. **t.II**, 48 (1879).
[3] J. K. Platten and P. Costesèque, Eur. Phys. J. E **15**, 235 (2004).
[4] P. C. Mangelsdrof, Jr., J. Chem. Phys. **32**, 293 (1960).
[5] D. Walker and S. E. DeLong, Contrib. Mineral. Petrol. **85**, 203 (1984).
[6] S. Wiegand, J. Phys.: Condens. Matter **16**, 357 (2004).
[7] M. Giglio and A. Vendramini, Phys. Rev. Lett. **34**, 561 (1975).
[8] R. Piazza and A. Guarino, Phys. Rev. Lett. **88**, 208302 (2002).
[9] E. Bringuier and A. Bourdon, Phys. Rev. E **67**, 011404 (2003).
[10] S. Fayolle, T. Bickel, S. Le Boiteux, and A. Würger, Phys. Rev. Lett. **95**, 208301 (2005).
[11] J. A. Bierlein, J. Chem. Phys. **23**, 10 (1955).
[12] J. K. Platten, J. Appl. Mech. **73**, 5 (2006).
[13] H. Ševčíková and M. Marek, Physica D **9**, 140 (1983).
[14] H. Ševčíková, M. Marek, and S. C. Müller, Science **257**, 951 (1992).
[15] S. Dutta and D. S. Ray, Phys. Rev. E **73**, 026210 (2006).
[16] Á. Tóth, I. Lagzi, and D. Horváth, J. Phys. Chem. **100**, 14837 (1996).
[17] F. Sagués and I. R. Epstein, Dalton Trans. **7**, 1201 (2003).
[18] S. Dutta, S. S. Riaz, and D. S. Ray, Phys. Rev. E **71**, 036216 (2005).
[19] A. Hanna, A. Saul, and K. Showalter, J. Am. Chem. Soc. **104**, 3838 (1982).
[20] D. Horváth and K. Showalter, J. Chem. Phys. **102**, 2471 (1995).
[21] J. H. Merkin and H. Ševčíková, Phys. Chem. Chem. Phys. **1**, 91 (1999).
[22] Stephen K. Scott, *Oscillations, Waves, and Chaos in Chemical Kinetics* (Oxford University Press, New York, 1994).
[23] G. Schmitz, Phys. Chem. Chem. Phys. **2**, 4041 (2000).
[24] I. R. Epstein and J. A. Pojman, *An Introduction to Nonlinear Chemical Dynamics* (Oxford University Press, New York, 1998).
[25] I. Prigogine, L. de Brouckère, and R. Amand, Physica (Amsterdam) **16**, 577 (1950).
[26] K. G. Denbigh, Trans. Faraday Soc. **48**, 1 (1952).
[27] J. Luettmer-Strathmann, e-print arXiv:cond-mat/0304615.
[28] J. R. Bamforth, S. Kalliadasis, J. H. Merkin, and S. K. Scott, Phys. Chem. Chem. Phys. **2**, 4013 (2000).
[29] R. Haase, *Thermodynamics of Irreversible Processes* (Addison-Wesley, Reading, MA, 1969).
[30] T. Völkera, E. Blumsb, and S. Odenbacha, J. Magn. Magn. Mater. **252**, 218 (2002).
[31] T. Mair, C. Wamke, K. Tsuji, and S. C. Müler, Biophys. J. **88**, 639 (2005).